

Resonant Chains of Exoplanets: Libration Centers for Three-body Angles

JARED C. SIEGEL¹ AND DANIEL FABRYCKY¹

¹*Department of Astronomy and Astrophysics, University of Chicago
5640 S Ellis Ave
Chicago, IL 60637, USA*

ABSTRACT

Resonant planetary systems contain at least one planet pair with orbital periods librating at a near-integer ratio (2/1, 3/2, 4/3, etc.) and are a natural outcome of standard planetary formation theories. Systems with multiple adjacent resonant pairs are known as resonant chains and can exhibit three-body resonances —characterized by a critical three-body angle. Here we study three-body angles as a diagnostic of resonant chains through tidally-damped N-body integrations. For each combination of the 2:1, 3:2, 4:3, and 5:4 mean motion resonances (the most common resonances in the known resonant chains), we characterize the three-body angle equilibria for several mass schemes, migration timescales, and initial separations. We find that under our formulation of the three-body angle, which does not reduce coefficients, 180° is the preferred libration center, and libration centers shifted away from 180° are associated with non-adjacent resonances. We then relate these angles to observables, by applying our general results to two transiting systems: Kepler-60 and Kepler-223. For these systems, we compare N-body models of the three-body angle to the zeroth order in e approximation accessible via transit phases, used in previous publications. In both cases, we find the three-body angle during the *Kepler* observing window is not necessarily indicative of the long-term oscillations and stress the role of dynamical models in investigating three-body angles. We anticipate our results will provide a useful diagnostic in the analysis of resonant chains.

Keywords: planetary systems — planets and satellites: dynamical evolution and stability — stars: individual (Kepler-60, Kepler-223)

1. INTRODUCTION

Standard theories of planet formation predict planetary migration to be pervasive. After planets are spawned in protoplanetary disks, they create gravitational wakes, which torque the planets' orbits (type-I migration, [Ward 1997](#)). Since the migration rate depends on the planetary mass, and moreover on the disk surface density and structure, as planets spiral in towards the star they can catch up to one another. Before overtaking each other, the planets interact strongly through resonant effects, which can transfer angular momentum among planets on a timescale even faster than the disk torques each planet. This effect gives rise to resonant trapping phenomena, in which planets migrate in lock-step, with near integer-ratio orbital periods. The

eventual draining and photoevaporation of the disk can leave behind resonant planets as a fossil record of this evolution.

Systems with multiple planet pairs each locked in a mean motion resonance (MMR) —where the pair's orbital periods librate at a near-integer ratio— are known as resonant chains. Simulations of planetary migration initially predicted such systems ([Cresswell & Nelson 2006](#)), and [Mills et al. \(2016\)](#) successfully reproduced the observed state of Kepler-223, a four planet resonant chain, using a gas-disk migration model. More recently, [MacDonald & Dawson \(2018\)](#) demonstrated multiple channels of migration —long-scale, short-scale, and pure eccentricity damping— are compatible with several observed chains.

There are now five confirmed exoplanet resonant chains, including systems composed of giants (GJ 876, [Rivera et al. 2010](#)), sub-Neptunes (Kepler-223, [Mills et al. 2016](#)), super-Earths with and without gas envelopes (Kepler-80 and TOI-178, [MacDonald et al. 2016](#);

Leleu et al. 2021), and terrestrials (TRAPPIST-1, Gillon et al. 2016; Luger et al. 2017). In addition, there are currently three suspected resonant chains: HR 8799 (Fabrycky & Murray-Clay 2010), Kepler-60 (Jontof-Hutter et al. 2016; Goździewski et al. 2016), and K2-138 (Christiansen et al. 2018; Lopez et al. 2019); however, Jontof-Hutter et al. (2016) was recently revised by Jontof-Hutter et al. (2021), showing the three-body angle of Kepler-60 indeed librates, potentially promoting this system to a confirmed resonant chain. Among all these systems, period ratios between adjacent planets are predominately near first-order commensurabilities, with the only higher-order commensurabilities (5:3 and 8:5) found in the inner two pairs of TRAPPIST-1. Other systems — e.g., HD 158259 (Hara et al. 2020) and Kepler-444 (Papaloizou 2016) — bear the resonant hallmarks of convergent migration, though they lack librating three-body resonances, described next.

1.1. Three-body Angles

In resonant systems, three-body resonances can engage and link the planets’ dynamics together. Such resonances are characterized by the general three-body angle, which is found through a linear-combination of the planets’ mean longitudes. These angles are easily detected in transit data, because they strongly rely on the observed transit phase (with a weak dependence on eccentricity) and are a powerful diagnostic of system architecture.

A general three-planet resonant chain obeys $\frac{P_2}{P_1} \approx \frac{j+1}{j}$ and $\frac{P_3}{P_2} \approx \frac{k+1}{k}$, where j, k are integers and P_i are the periods of subsequent planets ($i = 1, 2, 3$); we refer to such chains by $(j+1 : j, k+1 : k)$. For a given chain, the system can be characterized by the two critical angles:

$$\phi_{12} = (j+1)\lambda_2 - j\lambda_1 - \varpi_2 \quad (1)$$

$$\phi_{23} = (k+1)\lambda_3 - k\lambda_2 - \varpi_2 \quad (2)$$

where λ_i and ϖ_i are the mean longitudes and pericenter longitudes, respectively. Subtracting ϕ_{12} from ϕ_{23} then yields the general three-body angle:

$$\phi = j\lambda_1 - (j+k+1)\lambda_2 + (k+1)\lambda_3 \quad (3)$$

If both critical angles librate, it follows that ϕ will librate. This scenario, called type-I by Goździewski et al. (2016), is the primary focus of this paper; however, we note ϕ can librate even if all the two-body critical angles circulate.

Prior studies often reduce equation 3 by the greatest common denominator. Unless otherwise stated, we do not reduce the angles and use the formulation of equation 3.

1.2. Motivation and Overview

As the number of known resonant chains grows, it has typically fallen to complex transit-timing variation (TTV) analysis (Kepler-60, Migaszewski 2016; Jontof-Hutter et al. 2016), involved analytics (HR8799, Goździewski & Migaszewski 2020), or numerical modeling (Kepler-223 and TRAPPIST-1, Mills et al. 2016; Tamayo et al. 2017) to predict the three-body angles of observed systems.

Using a semi-analytic approach, Delisle (2017) developed a model of three-body angle equilibria and applied it to Kepler-223. Delisle (2017) found $\phi = 180^\circ$ in cases without first-order non-adjacent MMR and identified multiple equilibria otherwise. However, this model does not treat higher-order non-adjacent MMR and requires substantial mathematical machinery, limiting its applicability to observed systems.

In a method first employed by Mills et al. (2016) and generalized by Luger et al. (2017), the observed transit times can be mapped to mean longitudes, and by extension the three-body angle, using a zeroth order in e approximation. This approach is independent of dynamical modeling and treats the three-body angle as a direct observable, however, higher-order terms may be non-negligible.

Here we perform tidally-damped N-body integrations, in order to characterize the three-body angle equilibria for an array of resonant configurations; since the observed resonant chains predominately host planet pairs near first-order commensurabilities, we focus on combinations of the 2:1, 3:2, 4:3, and 5:4 MMRs. Motivated by the observed chains, we also focus on the super-Earth to sub-Neptune mass regime. Through these simulations and a standardized formulation of the three-body angle, we present a general rule for three-body angle equilibria. We then relate our numerical results with their observational equivalents, by conducting transit timing variation studies of Kepler-60 and Kepler-223.

In §2, we present the framework of our integrations and outline the simulations conducted in this study. Our numerical results are then presented in §3. In §4, we apply these results to observed systems, and in §5, we summarize our conclusions.

2. SIMULATIONS

Using tidally-damped N-body integrations, we characterize the three-body angle equilibria for an array of resonant configurations. Here we outline the methods of those integrations and summarize the simulation parameters.

2.1. Methods

Table 1. Simulation Parameters

Name	Mass Scheme (M_{\oplus})	τ_a (days)	K
Mass Expl.			
— \mathcal{S}_1	4.0, 4.0, 4.0	10^8	10^3
— \mathcal{S}_2	8.0, 8.0, 8.0	10^8	10^3
— \mathcal{S}_3	2.0, 4.0, 6.0	10^8	10^3
— \mathcal{S}_4	4.0, 6.0, 8.0	10^8	10^3
Timescale Expl.			
— \mathcal{S}_5	4.0, 4.0, 4.0	$10^6 - 10^9$	$5 - 10^3$

NOTE— For \mathcal{S}_1 through \mathcal{S}_5 , we generate models for all combinations of the 2:1, 3:2, 4:3, and 5:4 mean motion resonances. $t_1 = 1.46 \times 10^7$ days and $t_2 = 5.84 \times 10^7$ days for all integrations.

We follow the methods of [MacDonald et al. \(2016\)](#) and model Newtonian N-body dynamics using an 8th/9th order Prince-Dormand integration method from the GNU Scientific Library ([Galassi et al. 2009](#)). To simulate disk migration, we damp the semi-major axis (with a timescale of τ_a) of the outermost planet and eccentricity (with a timescale of τ_e) of every planet. Dissipation is implemented by applying an acceleration to dampen the radial and tangential velocities of individual planets with respect to the host star ([Thommes et al. 2008](#))¹

$$a_{\phi} = -v_{\phi}/(2\tau_a), \quad (4)$$

$$a_r = -2v_r/\tau_e, \quad (5)$$

where \vec{a} and \vec{v} are the acceleration applied to the planet and the planet’s instantaneous velocity, respectively, and their components are written with subscripts, referring to a polar coordinate system where r and ϕ are defined with respect to the central star. This scheme captures the planets sequentially into the resonances. Once each chain has captured into resonance and reached equilibrium eccentricity, the migration force is terminated at a time t_1 ; for every model in this study, we let $t_1 = 1.46 \times 10^7$ days. Our method brings several planets into resonance in a controlled fashion, though we are not attempting to model the likely physical situation of multiplanet migration near the inner edge of a gaseous disk, as others have done ([Brasser et al. 2018](#)); our particular choice can be related to the more general case,

¹ [Thommes et al. \(2008\)](#) mistakenly reported an extra $1/r$ factor in the a_r equation.

in which multiple planets have semi-major axis damping ([Rein et al. 2010](#)).

Following the migration phase, eccentricity damping is applied to each planet in accordance with tidal-damping, parameterized by the tidal-dissipation coefficient Q ([Goldreich & Soter 1966](#)), for a total time t_2 . In general, tidal-damping suppresses a given planet’s eccentricity e and spreads the period ratios away from commensurability. We relate the eccentricity-damping timescale to tidal-dissipation via the formulation of [Jackson et al. \(2008\)](#),

$$\frac{1}{\tau_e} = \frac{1}{e} \frac{de}{dt} = -\frac{63}{4} (GM_{\star})^{1/2} \frac{M_{\star}}{M_p} \frac{R_p^5}{a^{13/2}} \frac{1}{Q'} + \left(\frac{1}{e} \frac{de}{dt}\right)_{\star} \quad (6)$$

where Q' is defined as,

$$Q' = \frac{3Q}{2k_2}, \quad (7)$$

G is Newton’s gravitational constant, M_{\star} and M_p are the stellar and planetary masses, respectively, R_p is the planetary radius, k_2 is the Love number quantifying the susceptibility of a planet to tidal-distortion ([Papaloizou 2015](#)), and a is the semi-major axis. In equation 6, the term $\left(\frac{1}{e} \frac{de}{dt}\right)_{\star}$ denotes the dissipation effect of tides raised on the star; since we are focusing on very low-mass planets, we omit that portion in our analysis.

Unless otherwise stated, we assume Q' is constant among all planets in a system and set Q' such that the eccentricity-damping timescale of the innermost planet is ten-times longer in the tidal-damping phase than the migration phase. The eccentricity-damping of the outer planets scale according to equation 6, assuming uniform planet radii.

2.2. Simulation Parameters

In order to characterize the three-body angle equilibria, we generate and integrate synthetic systems for each chain of the form $(j + 1 : j, k + 1 : k)$, where $j, k \in \{1, 2, 3, 4\}$. For clarity, we group our models into two sets: mass exploration and timescale exploration. For the mass exploration suites, we are interested in mapping out the resonant equilibria of each configuration and comparing between four different planet mass schemes. With the timescale exploration suite, we investigate the sensitivity of these equilibria to a wide range of migration timescales and initial positions. Both sets are explained in detail below and summarized in Table 1.

For a given mass scheme in our mass exploration, we produce 30 simulations for each resonant configuration, initialize the planets on coplanar, circular orbits, 1% wide of their assigned commensurability, and draw each

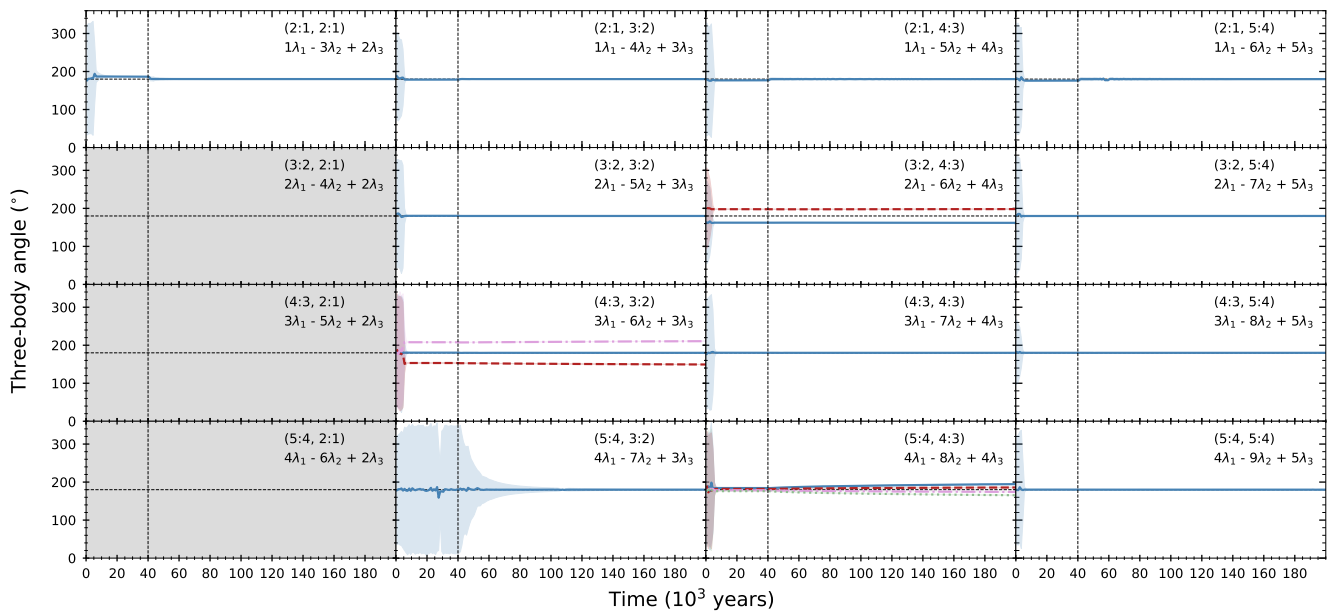


Figure 1. Evolution of the three-body angles in \mathcal{S}_1 , where $\tau_a = 10^8$ days and $K = 10^3$; the three-body angles are dependent on the adopted migration timescales (see §3.2). For each resonant configuration, the 30 models are grouped based on their three-body angle. The mean libration center of each group is represented as a line, the mean libration amplitude is shown as a shaded region, and the colors correspond to the different groups. The vertical dashed-black line demarcates the end of the migration regime and the start of the tidal-dissipation forces. Configurations without any libration of the three-body angle are shaded grey.

planet’s initial longitude from a uniform distribution between 0 and 2π . We produce four simulation suites of this form, each corresponding to a different planet mass scheme (labeled \mathcal{S}_1 , \mathcal{S}_2 , \mathcal{S}_3 , and \mathcal{S}_4 in Table 1). The mass schemes include two equal mass and two hierarchical configurations; these schemes are motivated by Weiss et al. (2018), which demonstrated general uniformity in a system’s planet sizes and identified outer planets as statistically larger in systems of three or more planets. For each model, we fix the stellar mass ($0.93 M_\odot$) and initial period of the inner planet (7.1320 days), as well as t_1 and t_2 , the lengths of the migration and tidal-damping phases, respectively. To ensure all systems capture into their assigned MMR, we set $\tau_a = 10^8$ days and $K = 10^3$, where $K \equiv \tau_a/\tau_e$; we explore the effects of changing the migration timescales in §3.2. These parameters are summarized in Table 1.

In our timescale investigation, we produce models on a grid of τ_a and K values for each resonant configuration; we assign twenty-two τ_a values between 10^6 and 10^9 days and twenty-two K values between 5 and 10^3 , both in logarithmic spacing. Each planet’s orbital elements are chosen as above, except that initial orbital periods are drawn from a uniform distribution between 0.5% and 5% wide of the assigned commensurability. The stellar

mass, innermost orbital period, and t_1, t_2 are unchanged from the mass exploration suites (\mathcal{S}_1 through \mathcal{S}_4). For the planet masses, we adopt the 4.0, 4.0, 4.0 M_\oplus scheme from \mathcal{S}_1 . These models are summarized in Table 1 and designated \mathcal{S}_5 .

3. SIMULATION RESULTS

From our numerical integrations, we find 180° is the preferred libration center for nearly all three-body angles. The notable exceptions are the (3:2, 4:3), (4:3, 3:2), and (5:4, 4:3) configurations, where the three-body angle admits equilibria off 180° ; we discuss these three configurations in detail in §3.3.

To illustrate this behavior, in Figure 1 we present the evolution of the three-body angle equilibria for \mathcal{S}_1 (see Table 1 for model parameters). We also report the libration center and amplitude for each equilibria in Table 2, again for \mathcal{S}_1 . The reported values are taken from a 1 kyr window beginning when the inner period ratio has spread 0.5% from the assigned commensurability. With the exception of the (5:4, 4:3) chain, we find the three-body angle does not evolve considerably with additional spreading.

In \mathcal{S}_1 , we find that for three resonant configurations — (3:2, 2:1), (4:3, 2:1), and (5:4, 2:1)— the three-body

Table 2. Three-body Angle Equilibria for \mathcal{S}_1

P_2/P_1	P_3/P_2	Three-body Angle	Center ($^\circ$)	Amplitude ($^\circ$)	Fraction
2:1	2:1	$1\lambda_1 - 3\lambda_2 + 2\lambda_3$	180.08 ± 0.01	0.03 ± 0.03	30/30
2:1	3:2	$1\lambda_1 - 4\lambda_2 + 3\lambda_3$	180.03 ± 0.02	0.14 ± 0.11	30/30
2:1	4:3	$1\lambda_1 - 5\lambda_2 + 4\lambda_3$	180.01 ± 0.03	0.09 ± 0.26	30/30
2:1	5:4	$1\lambda_1 - 6\lambda_2 + 5\lambda_3$	179.98 ± 0.06	1.36 ± 0.04	30/30
3:2	2:1	$2\lambda_1 - 4\lambda_2 + 2\lambda_3$	—	—	30/30
3:2	3:2	$2\lambda_1 - 5\lambda_2 + 3\lambda_3$	180.02 ± 0.05	0.07 ± 0.05	30/30
3:2	4:3	$2\lambda_1 - 6\lambda_2 + 4\lambda_3$	162.00 ± 0.12	0.27 ± 0.07	11/30
			197.90 ± 0.10	0.21 ± 0.12	19/30
3:2	5:4	$2\lambda_1 - 7\lambda_2 + 5\lambda_3$	180.00 ± 0.02	0.63 ± 0.02	30/30
4:3	2:1	$3\lambda_1 - 5\lambda_2 + 2\lambda_3$	—	—	30/30
4:3	3:2	$3\lambda_1 - 6\lambda_2 + 3\lambda_3$	148.73 ± 0.01	0.24 ± 0.03	7/30
			180.00 ± 0.03	0.28 ± 0.02	16/30
			211.29 ± 0.02	0.25 ± 0.03	7/30
4:3	4:3	$3\lambda_1 - 7\lambda_2 + 4\lambda_3$	180.00 ± 0.01	0.41 ± 0.02	30/30
4:3	5:4	$3\lambda_1 - 8\lambda_2 + 5\lambda_3$	180.00 ± 0.03	0.73 ± 0.06	30/30
5:4	2:1	$4\lambda_1 - 6\lambda_2 + 2\lambda_3$	—	—	30/30
5:4	3:2	$4\lambda_1 - 7\lambda_2 + 3\lambda_3$	180.02 ± 0.06	0.45 ± 0.36	30/30
5:4	4:3	$4\lambda_1 - 8\lambda_2 + 4\lambda_3$	166.41 ± 0.02	0.58 ± 0.06	6/30
			174.54 ± 0.03	0.79 ± 0.02	12/30
			185.42 ± 0.03	0.78 ± 0.03	7/30
			193.58 ± 0.01	0.64 ± 0.05	5/30
5:4	5:4	$4\lambda_1 - 9\lambda_2 + 5\lambda_3$	180.00 ± 0.03	1.00 ± 0.06	30/30

angle circulates. This is not universal for these chains and is a consequence of the selected τ_a and τ_e for \mathcal{S}_1 through \mathcal{S}_4 . As discussed in §3.2, when different migration timescales are adopted, all three of these chains admit librating solutions with $\phi = 180^\circ$. Unless otherwise stated, librating solutions refer to systems in which the three-body angle librates; as stated in §1, libration of the three-body angle does not guarantee libration of the two-body angles.

For the resonant equilibria reported in Figure 1 and Table 2, the three-body angles are found by the formulation of §1.1 and the libration amplitudes are given by (Millholland et al. 2018),

$$A = \sqrt{\frac{2}{N} \sum_{i=1}^N (\phi_i - \bar{\phi})^2} \quad (8)$$

which approximates the amplitude of sinusoidal oscillations over a sample of ϕ ; i indexes over the time-steps, N is the number of time-steps, and $\bar{\phi}$ is the mean of the sample.

We next investigate the sensitivity of these equilibria to different mass schemes (§3.1) and migration

timescales (§3.2), as well as discuss the off 180° equilibria (§3.3) and cases of three-body angle circulation (§3.4).

3.1. Mass Dependency

By comparing the three-body angle equilibria of \mathcal{S}_1 through \mathcal{S}_4 , we investigate the sensitivity of the equilibria to planet masses. In general, the three-body angles of \mathcal{S}_1 , \mathcal{S}_2 , \mathcal{S}_3 , and \mathcal{S}_4 are highly similar. We again find that 180° is the preferred libration center and identify shifts about 180° in the same three resonant configurations. In Table 3, we compare the libration centers and libration amplitudes for the chains not centered at 180° between the four mass schemes. For ease of comparison, the reported values are again taken from a 1 kyr window beginning when the inner period ratio has spread 0.5% from the assigned commensurability. The effects of varying the mass scheme are minimal; the differences in amplitude are all less than 1° and the differences in libration center are less than 5° . For the super-Earth to sub-Neptune regime, shifts in the three-body angle due to planet masses are thus considerably less significant than those induced by non-adjacent resonances.

Table 3. Three-body Angle Mass Dependency

P_2/P_1	P_3/P_2	$\bar{\phi}^{(\mathcal{S}_1)} - \bar{\phi}^{(\mathcal{S}_2)}$	$A^{(\mathcal{S}_1)} - A^{(\mathcal{S}_2)}$	$\bar{\phi}^{(\mathcal{S}_1)} - \bar{\phi}^{(\mathcal{S}_3)}$	$A^{(\mathcal{S}_1)} - A^{(\mathcal{S}_3)}$	$\bar{\phi}^{(\mathcal{S}_1)} - \bar{\phi}^{(\mathcal{S}_4)}$	$A^{(\mathcal{S}_1)} - A^{(\mathcal{S}_4)}$
3:2	4:3	0.33 ± 0.24	-0.13 ± 0.22	-0.18 ± 0.12	-0.09 ± 0.07	0.03 ± 0.12	-0.22 ± 0.08
		-0.38 ± 0.27	-0.34 ± 0.18	0.11 ± 0.11	-0.16 ± 0.12	-0.08 ± 0.11	-0.27 ± 0.12
4:3	3:2	0.71 ± 0.03	-0.24 ± 0.05	0.13 ± 0.01	0.12 ± 0.12	0.32 ± 0.01	-0.07 ± 0.03
		-0.01 ± 0.03	-0.24 ± 0.02	-0.01 ± 0.03	0.05 ± 0.02	-0.01 ± 0.03	-0.08 ± 0.02
		-0.71 ± 0.02	-0.25 ± 0.04	-0.11 ± 0.02	0.06 ± 0.03	-0.34 ± 0.02	-0.06 ± 0.03
5:4	4:3	-0.39 ± 0.08	-0.59 ± 0.15	-2.98 ± 4.29	0.01 ± 0.13	-0.08 ± 0.07	-0.18 ± 0.09
		-0.04 ± 0.06	-0.70 ± 0.05	-0.06 ± 0.04	0.08 ± 0.04	0.01 ± 0.25	-0.22 ± 0.07
		0.33 ± 0.29	-0.63 ± 0.10	0.01 ± 0.04	0.07 ± 0.03	0.05 ± 0.05	-0.27 ± 0.03
		-0.98 ± 3.33	-0.53 ± 0.13	-1.44 ± 3.33	0.21 ± 0.18	-1.30 ± 3.33	-0.11 ± 0.08

NOTE—The three-body angle equilibria are presented in the same order as Table 2, and suites \mathcal{S}_1 through \mathcal{S}_4 are described in Table 1.

Table 4. Three-body Angle Equilibria for \mathcal{S}_5 (see Table 1 for comparison)

Resonant Configuration	Libration Center ($^\circ$)
(3:2, 4:3)	162.08 ± 0.60
	197.88 ± 0.49
(4:3, 3:2)	148.80 ± 0.11
	180.01 ± 0.39
	211.41 ± 0.27
(5:4, 4:3)	167.24 ± 0.78
	173.56 ± 2.30
	185.52 ± 1.88
	192.56 ± 0.67
Others	180.09 ± 0.42

We note two significant differences across the suites. Firstly, in the two hierarchical configurations (\mathcal{S}_3 and \mathcal{S}_4), the three-body angle for the (3:2, 2:1) chain librates in all 30 models about $\phi = 180^\circ$, while it does not librate in any of the models for the two equal-mass suites (\mathcal{S}_1 and \mathcal{S}_2). Secondly, in the (5:4, 3:2) and (5:4, 5:4) chains, we find that only a fraction of the models librate in the three additional mass schemes (\mathcal{S}_2 , \mathcal{S}_3 , and \mathcal{S}_4), even though all the models librate in the 4.0, 4.0, 4.0 M_\oplus scheme.

As such, we find the equilibria positions are weakly dependant on the mass scheme, but whether the system librates or circulates can strongly depend on the mass scheme.

3.2. Migration Timescale Dependency

Using \mathcal{S}_5 , we next explore the three-body angle equilibria for an array of migration timescales and initial positions. For each resonant configuration, we integrate synthetic systems for a grid of τ_a and K values, with the initial orbital periods drawn from a uniform distribution between 0.5% and 5% wide of the assigned commensurability.

In Table 4, we report the libration centers for all systems that capture into their assigned commensurability and achieve steady-state by the end of the migration phase. As in Tables 2 and 3, the reported values are taken from a 1 kyr window beginning when the inner period ratio has spread 0.5% from the assigned commensurability.

We find agreement between the libration centers reported in Table 4 and those presented in Table 2, indicating a weak dependence between the three-body angle equilibria and the migration timescales. However, we do not anticipate an exact match, since the range of τ_e values for \mathcal{S}_5 allows for larger libration amplitudes, and by extension, greater scatter in the reported three-body angles.

3.3. Off 180° Equilibria

Across our models, we find 180° is the preferred equilibria for the three-body angle, with the exception of three resonant configurations: (3:2, 4:3), (4:3, 3:2), and (5:4, 4:3).

In the (3:2, 4:3) and (4:3, 3:2) chains, the deviations from 180° occur at the moment libration begins and show little evolution in the tidal-dissipation regime. From Tables 2 and 4, we find the shifts are symmetric about 180° for a wide range of migration timescales and initial conditions. This behavior was predicted by

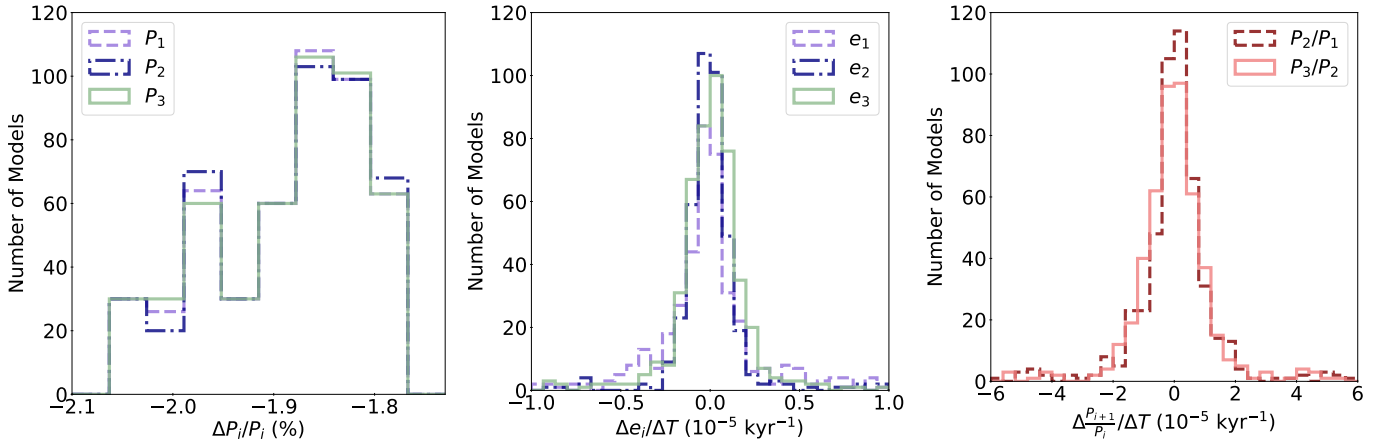


Figure 2. Demonstration that all systems in \mathcal{S}_1 through \mathcal{S}_4 , including those not librating, reach a steady-state during the last 10 kyr of migration. *Left:* the percent change in orbital period for each planet over the last 10 kyr of migration. *Middle:* the rate of change in eccentricity for each planet over the same 10 kyr. *Right:* the rate of change in the period ratios, again over the last 10 kyr of migration.

Delisle (2017), because for both configurations there is a first-order non-adjacent MMR, $P_3 : P_2 \approx 2 : 1$.

Unlike the (3:2, 4:3) and (4:3, 3:2) chains, shifts in the three-body angle for the (5:4, 4:3) configuration do not fully present themselves until the tidal-dissipation regime; however, these libration centers still obey the near-symmetry about 180° . Since $P_3 : P_2 \approx 5 : 3$, this behavior was not considered by the semi-analytic model of Delisle (2017), which was limited to first-order non-adjacent MMR.

Prompted by the (5:4, 4:3) chain, where the three-body angles continue spreading in the tidal-dissipation regime, we repeat \mathcal{S}_1 for the (3:2, 4:3), (4:3, 3:2), and (5:4, 4:3) chains using a range of Q' values. Consistent with Papaloizou (2015), we find that lowering the assumed Q' value by an order of magnitude corresponds to an order of magnitude speedup in the evolution. In the lower Q' suites, the three-body angles of the (3:2, 4:3), (4:3, 3:2), and (5:4, 4:3) chains all clearly spread in the tidal-dissipation regime, while only the (5:4, 4:3) configuration visibly spreads in Figure 1. The effect is strongest in the (5:4, 4:3) chain and significantly weaker in the (3:2, 4:3) and (4:3, 3:2) chains.

Thus, we are able to expand upon the semi-analytic findings of Delisle (2017) and conclude that not only are higher-order non-adjacent resonances capable of off 180° equilibria, but their dependence on tidal-damping appears significantly amplified. As a result, for systems near a (5:4, 4:3) chain, such as Kepler-60, the three-body angle can occupy a range of values, depending on the evolutionary history of the system, see §4.2 for discussion.

3.4. Non-librating Three-body Angles

Although a full investigation into the systems with non-librating three-body angles is beyond the scope of this paper, here we briefly discuss the parameters that influence the libration state of the three-body angle and compare the migration histories of the librating and non-librating populations.

In §3.1, we found the libration state of the three-body angle depends strongly on the mass scheme. Additionally, we found that for each resonant configuration, certain regions of the τ_a and K space admit librating solutions, while others admit circulating ones (§3.2). Given the stochastic nature of this parameter space, the large number of resonant configurations, and the strong mass dependence, we refrain from characterizing these regions of libration and circulation and leave this analysis to future work.

We also find that for the systems with non-librating three-body angles in \mathcal{S}_1 through \mathcal{S}_4 , each planet still captures into its assigned commensurability and reaches eccentricity-equilibrium by t_1 . This is evidenced by Figure 2, where we present the change in the periods, period ratios, and eccentricities over the final 10 kyr of the migration phase for all models in \mathcal{S}_1 through \mathcal{S}_4 ; the eccentricity and period ratio distributions are both consistent with zero, while the periods themselves are shrinking. This confirms the planets are migrating in lock-step, even for the systems with circulating three-body angles.

4. APPLICATION

In transit data, three-body angles are often nontrivial to extract, complicating the application of our results to observed systems. Prior studies have often turned to forward integration of transit timing variation (TTV) solutions (Goździewski et al. 2016; MacDonald et al. 2016; Jontof-Hutter et al. 2016), or considered the zeroth order in e approximation of Mills et al. (2016) and Luger et al. (2017).

Here, we first derive this approximation and then use this method, along with forward integration of TTV solutions, to compare the three-body angles of Kepler-60 and Kepler-223 with the results of §3. For Kepler-60, we find the TTV solutions agree with our results and suggest the system has undergone minimal tidal-dissipation, while for Kepler-223, we update the three-body angles reported in Mills et al. (2016). For both systems, we discuss the quality of the zeroth order in e approximation of ϕ as a diagnostic of the three-body angle.

4.1. Three-body Angles from TTV Data

A transit time T can be related to a mean anomaly λ , by noting that the value of the true anomaly f at mid-transit obeys $f + \omega = \pi/2$; this means the line between the star and the planet has swept $\pi/2$ from crossing the sky plane to the time of mid-transit². The relation between f and time is, to second order in e (Murray & Dermott 1999, eq. 2.88, 2.93):

$$f = M + 2e \sin M + (5/4)e^2 \sin 2M, \quad (9)$$

$$M = f - 2e \sin f + (3/4)e^2 \sin 2f, \quad (10)$$

where $M = \lambda - \varpi$. Here we are setting $\Omega = 0$, so $\varpi = \omega$. We may then take equation 10 and trigonometric identities to determine λ at the mid-time of a transit:

$$\lambda_t = \pi/2 - 2e \cos \omega + 3/4e^2 \sin 2\omega, \quad (11)$$

$$\lambda_t = \pi/2 - 2(e \cos \omega) + 3/2(e \sin \omega)(e \cos \omega), \quad (12)$$

again to second-order in eccentricity. Since λ_t is a *mean* longitude, which progresses linearly in time, we may express it as a function of transit time and period:

$$\lambda_t = \frac{\pi}{2} + 2\pi \frac{t - T_n}{P} - 2e \cos \omega + \frac{3}{2}(e \sin \omega)(e \cos \omega) \quad (13)$$

² The appendix of Hamann et al. (2019) showed that when the planet is eccentric and inclined from edge-on, an additional term $\Delta T/P \propto (i - \pi/2)^2 e \cos \omega$ is needed, which we neglect here.

Combining for all three planets, we have:

$$\phi_{\text{ttv}} = 2\pi \left(j \frac{t - T_1}{P_1} - (j + k + 1) \frac{t - T_2}{P_2} + (k + 1) \frac{t - T_3}{P_3} \right) \quad (14)$$

$$\begin{aligned} \phi - \phi_{\text{ttv}} = & j(-2e_1 \cos \omega_1 + \frac{3}{2}e_1^2 \sin \omega_1 \cos \omega_1) \\ & - (j + k + 1)(-2e_2 \cos \omega_2 + \frac{3}{2}e_2^2 \sin \omega_2 \cos \omega_2) \\ & + (k + 1)(-2e_3 \cos \omega_3 + \frac{3}{2}e_3^2 \sin \omega_3 \cos \omega_3) \\ & + \mathcal{O}(e_1^3, e_2^3, e_3^3). \end{aligned} \quad (15)$$

where ϕ_{ttv} is the three-body angle inferred using λ_t to zeroth order in e , ϕ is defined in equation 3, and j, k are defined as in §1. Previous publications (e.g., Luger et al. 2017) took $e \rightarrow 0$ and only considered ϕ_{ttv} , since there is no easy observational access to e and ω , like there is for T and P . However, since we are interested in comparing the three-body angles of transiting systems with our synthetic systems, we also consider the higher order correction $\phi - \phi_{\text{ttv}}$.

4.2. Kepler-60

Kepler-60 hosts three transiting super-Earths with periods near a chain of first-order commensurabilities, 5:4 for the inner pair and 4:3 for the outer pair (Steffen et al. 2013). Through forward integration of TTV solutions, Goździewski et al. (2016) suggested the system's three-body angle was librating and the two-body angles were likely librating as well. According to a recent erratum, Jontof-Hutter et al. (2021) also found the TTVs implied a librating three-body angle. Both studies quote a libration center of $\sim 45^\circ$; our standard three-body angle definition multiplies their definition by 4, corresponding to $\phi \approx 180^\circ$ with an amplitude of 20° .

Using three dynamical histories—long-scale migration, short-scale migration, and pure eccentricity damping—MacDonald & Dawson (2018) simulated the formation of Kepler-60 and found four equilibria for the three-body angle, none of which are consistent with $\phi = 180^\circ$; in our standard formulation, these equilibria are approximately $164.52 - 178.72^\circ$, $176.52 - 179.36^\circ$, $180.12 - 185.64^\circ$, and $182.36 - 189.92^\circ$. We find general agreement between our results for the (5:4, 4:3) configuration and the modeling by MacDonald & Dawson (2018), but given the significant dependence of the libration centers on tidal-dissipation in the (5:4, 4:3) chains (see §3.3) and the range of damping timescales employed by MacDonald & Dawson (2018), we do not expect an exact match.

We revisit the 50 samples described in Jontof-Hutter et al. (2016, section 3.5), available via Jontof-Hutter

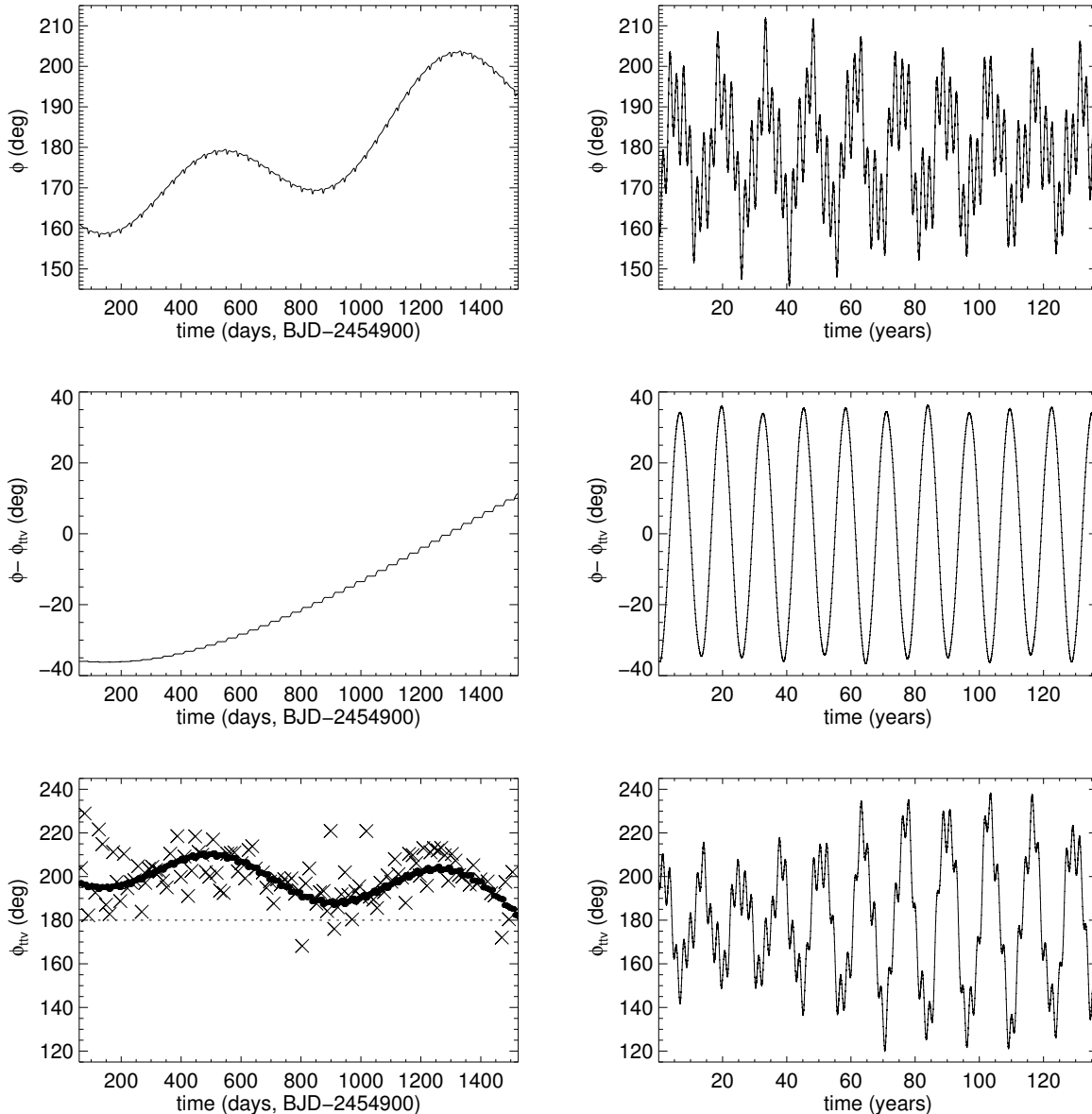


Figure 3. The evolution of Kepler-60’s three-body angle over time, from a fit to the data (Jontof-Hutter et al. 2021). In the top two panels, the exact three-body angles are displayed, over the course of the data and over the next 137 years. In the middle panels, the difference between the true angles and the transit-identifiable angles is shown. In the bottom panels, the transit-identifiable angles (i.e., Luger et al. 2017, and eqn. 14 of this paper) are shown. The values from the transit-timing data are overplotted in the bottom-left panel, measured at planet d’s transit times using the closest transits of planets b and c. An apparent libration around 200° is illusory, due to short-timescale fluctuations; the long-term behavior in the bottom-right panel shows the expected libration near 180° (actually 179.12° , due to the 5:3 resonance between planets b and d).

et al. (2021), integrating them 1000 years from the start of the Kepler data ($t = 0$ is BJD 2454900), to infer ϕ . We analyze an interval between $t = 100$ yr and 1000 yr, so that the phase of ϕ loses coherence among the various samples from their starting condition fitting the data. We find an average value of $\phi = 179.12^\circ \pm 0.10^\circ$, with a well-constrained amplitude of $17.5^\circ \pm 2.9^\circ$.

As shown in Figure 1, our synthetic systems predict the three-body angle of the (5:4, 4:3) configuration spreads from 180° through tidal-dissipation. We verified that the value of 179.12° measured from the data posterior above is typical of the centers observed in S_5 when the period ratios match that of the observed system.

From the match between theory and observation for the libration center of ϕ , we conclude Kepler-60 has un-

dergone limited tidal-damping. This agrees with [Papaloizou \(2015\)](#), which estimated $Q' \gtrsim 67,000$.

Using TTV data from [Rowe et al. \(2015\)](#), we present the zeroth order in e three-body angle of Kepler-60 in Figure 3. We find this zeroth order approximation of ϕ seems to librate around 200° , with an amplitude of 10° . Thus, over the *Kepler* observing window, the libration center of the zeroth order ϕ appears discrepant with our models (see Table 2) and the TTV forward integrations of [Goździewski et al. \(2016\)](#) and [Jontof-Hutter et al. \(2021\)](#). However, since the system is only slightly wide of near-integer ratios, we expect the higher-order corrections in e to be non-negligible. For Kepler-60, the first-order in e correction is:

$$-8e_b \cos \omega_b + 16e_c \cos \omega_c - 8e_d \cos \omega_d \quad (16)$$

and the second-order error term is:

$$\begin{aligned} &6(e_b \cos \omega_b)(e_b \sin \omega_b) \\ &-12(e_c \cos \omega_c)(e_c \sin \omega_c) \\ &+6(e_d \cos \omega_d)(e_d \sin \omega_d). \end{aligned} \quad (17)$$

In Figure 3, we present the exact three-body angle (ϕ) and the difference between ϕ and the zeroth order approximation ($\phi - \phi_{ttv}$) for a single draw from the posterior ([Jontof-Hutter et al. 2016](#); [Jontof-Hutter et al. 2021](#)). The apparent libration near 200° just reflects short-period components of the total oscillation. Meanwhile, the corrector term librates with a period of ~ 30 yr and an amplitude of 30° . From this forward integration, it appears the *Kepler* observing window was coincident with a near maximal discrepancy between the exact three-body angle and the zeroth order approximation.

Although both ϕ and ϕ_{ttv} agree with our models on longer timescales (> 15 yr), for an arbitrary 1500 day observing window this is not guaranteed. On such short timescales, the discrepancy between $\bar{\phi}$ and $\bar{\phi}_{ttv}$ may be non-negligible and neither angle may reflect their true libration centers. We thus urge caution when comparing the zeroth order approximation from TTV data to either our results or the semi-analytical solutions of [Delisle \(2017\)](#).

4.3. *Kepler-223*

Kepler-223 hosts four transiting planets with periods near a (4:3, 3:2, 4:3) resonant chain ([Rowe et al. 2014](#)). Using the zeroth order approximation outlined in §4.1, [Mills et al. \(2016\)](#) reported libration in $\phi_{1,ttv,M16}$ between 173° and 190° and in $\phi_{2,ttv,M16}$ between 47° and 75° ; under our standard formulation, $\phi_{1,ttv,M16}$ is multiplied by -3 and $\phi_{2,ttv,M16}$ is multiplied by 2 , corresponding to $150^\circ - 201^\circ$ and $94^\circ - 150^\circ$, respectively.

Using the same formulations as [Mills et al. \(2016\)](#), [Delisle \(2017\)](#) predicted six equilibria for Kepler-223, including the values reported by [Mills et al. \(2016\)](#). Unlike our three-planet models, where at most one non-adjacent resonant pair was possible, the (4:3, 3:2, 4:3) resonance configuration of Kepler-223 introduces two pairs of first-order resonances between non-adjacent planets — $P_d : P_b \approx 2 : 1$ and $P_e : P_c \approx 2 : 1$ — as well as a higher-order resonance between non-adjacent planets — $P_e : P_b \approx 8 : 3$. Under the [Delisle \(2017\)](#) model, these resonances result in numerous stable equilibria. The closest equilibria to the ϕ_{ttv} reported by [Mills et al. \(2016\)](#), translated into our parameters, is $\phi_1 = 168^\circ$ and $\phi_2 = 130^\circ$ ([Delisle 2017](#)).

Here, recognizing from equation 15 that there may be a significant offset between ϕ and ϕ_{ttv} due to eccentricity, we revisit the Kepler-223 analysis. In [Mills et al. \(2016\)](#) Extended Data Figure 5, it is shown that not all the systems that fit the data are stable, and not even all the ones that had been selected for 100 year ϕ libration (prior \mathcal{C}_3) maintain the property that is so characteristic of the system: that period ratios lie within ~ 0.001 of an integer ratio. In particular, from the quarter-to-quarter timing analysis, the period ratios of adjacent pairs fall in the ranges $P_c/P_b \in [1.3326, 1.3341]$, $P_d/P_c \in [1.5007, 1.5025]$, and $P_e/P_d \in [1.3331, 1.3346]$. To enforce that we are studying the ϕ behavior of systems that stay comparably close to integer ratios, we inspect the 2,008 runs that show stability for at least 1 Myr, from a draw of 5,000 systems fitting the data (the \mathcal{C}_2 prior). We compute the fraction of time that all three period ratios are in the above ranges (we allow P_d/P_c to go down to 1.500), i.e. very close to commensurability. A bimodality exists, in which 99.3% of the systems are this close to commensurability less than 18% of the time, with period ratios typically straying $\gtrsim 0.2\%$ from commensurability; 0.7% of the systems, just 14 of the 2,008, stay in these ranges $> 29\%$ of the time.

Thus we would expect that if the period ratios of Kepler-223 really do wander, and are found so close to commensurability during the Kepler observations by chance, then $\gtrsim 5$ “clones” of the system would be found with period ratios within $\sim 0.5\%$ of commensurability, but not within the bounds above. Recently, [Jiang et al. \(2020\)](#) curated a list of near resonant systems from *Kepler*, however, none of them are consistent with this characterization. This population consideration justifies the selection of only the systems that maintain period ratios very close to integer ratios.

With our selected data-fitting and stable systems, that maintain small period ratio variations, we find the li-

bration center and amplitude (equation 8) of each ϕ , over 10^6 years: $\phi_1 = 165_{-5}^{+11}$ °, $A_1 = 17_{-3}^{+8}$ ° and $\phi_2 = 133_{-7}^{+15}$ °, $A_2 = 30_{-10}^{+68}$ °. These central values are the median of the 14 values, and the error bars are the distance to the second and second-to-last values of the ordered set of 14 values, approximately $1\text{-}\sigma$. These results depend on the dynamical model of the system, so it should not be surprising that they substantially agree with Delisle (2017), based on the values quoted above.

The motivation for defining ϕ_{ttv} is that no dynamical model needs to be invoked, so it is a nearly direct observable. However, there are higher order in e corrections that should be estimated from the dynamical models (equation 15). For the set of 14 selected systems, the correction for ϕ_1 scans from $\sim -40^\circ$ at the start of the Kepler dataset to $\sim 5^\circ$ at the end and from $\sim 10^\circ$ to -25° for ϕ_2 . These values are larger than the errors quoted above, therefore we point out the importance of consulting dynamical models when determining ϕ , rather than relying solely on ϕ_{ttv} , despite its utility in being observable and easily computed.

5. CONCLUSIONS

Using tidally-damped N-body integrations, we characterized the three-body angle equilibria in compact three-planet systems for each combination of the 2:1, 3:2, 4:3, and 5:4 mean motion resonances (MMRs). We conducted this survey over an array of planet mass schemes, migration timescales, and initial separations. We then related these results to two transiting systems—Kepler-60 and Kepler-223—through transit timing variation (TTV) analysis.

We found that under our formulation of the three-body angle, which does not reduce the coefficients of equation 3, 180° is the preferred libration center and low-order, non-adjacent MMRs result in shifts about 180° , specifically in the (3:2, 4:3), (4:3, 3:2), and (5:4, 4:3) chains. In the chains with off 180° libration centers, we also identified a relationship between the three-body angle and tidal-dissipation effects; this relation is

strongest in the (5:4, 4:3) chain and is thus not characterized under the semi-analytic model of Delisle (2017), which was restricted to first-order non-adjacent resonances. An exploration of this behavior is beyond the scope of this work, however, we encourage future study of this relationship.

Through TTV analysis of Kepler-60 and Kepler-223, we considered the application of our results to transiting exoplanet systems. Comparison of the forward integrated TTV solutions with our results revealed that Kepler-60 has likely undergone minimal tidal-dissipation, consistent with the Q' estimation of Papaloizou 2015. For both systems, we found that on short timescales the zeroth order in e approximation for the three-body angle (see Mills et al. 2016; Luger et al. 2017) may be significantly discrepant from the three-body angles inferred via forward integration. As such, we stress the importance of consulting dynamical models when investigating three-body angles and caution against comparison of ϕ_{ttv} , the zeroth order approximation, to either our results or the models of Delisle (2017).

We propose that our results provide a simple diagnostic of observed three-body angles and should guide future use of ϕ_{ttv} .

ACKNOWLEDGMENTS

We thank the referee for their comments, which have helped to substantially improve the paper. We thank Daniel Jontof-Hutter, for helping us examine the Kepler-60 system, and Jack Lissauer, for discussing the long-term periods of Kepler-223. This work was completed in part with resources provided by the University of Chicago Research Computing Center. DF thanks former research assistants Kathryn Chapman, Sean Mills, and Enid Cruz-Colón for their work on resonant chains. JS thanks the Hoeft College Research Fellowship at the University of Chicago, for financial support.

REFERENCES

- Brasser, R., Matsumura, S., Muto, T., & Ida, S. 2018, ApJL, 864, L8, doi: [10.3847/2041-8213/aada18](https://doi.org/10.3847/2041-8213/aada18)
- Christiansen, J. L., Crossfield, I. J. M., Barentsen, G., et al. 2018, AJ, 155, 57, doi: [10.3847/1538-3881/aa9be0](https://doi.org/10.3847/1538-3881/aa9be0)
- Cresswell, P., & Nelson, R. P. 2006, A&A, 450, 833, doi: [10.1051/0004-6361:20054551](https://doi.org/10.1051/0004-6361:20054551)
- Delisle, J. B. 2017, A&A, 605, A96, doi: [10.1051/0004-6361/201730857](https://doi.org/10.1051/0004-6361/201730857)
- Fabrycky, D. C., & Murray-Clay, R. A. 2010, ApJ, 710, 1408, doi: [10.1088/0004-637X/710/2/1408](https://doi.org/10.1088/0004-637X/710/2/1408)
- Galassi, M., Davies, J., Theiler, J., et al. 2009, URL <http://www.gnu.org/s/gsl>, 103

- Gillon, M., Jehin, E., Lederer, S. M., et al. 2016, *Nature*, 533, 221, doi: [10.1038/nature17448](https://doi.org/10.1038/nature17448)
- Goldreich, P., & Soter, S. 1966, *Icarus*, 5, 375, doi: [10.1016/0019-1035\(66\)90051-0](https://doi.org/10.1016/0019-1035(66)90051-0)
- Goździewski, K., & Migaszewski, C. 2020, *ApJL*, 902, L40, doi: [10.3847/2041-8213/abb881](https://doi.org/10.3847/2041-8213/abb881)
- Goździewski, K., Migaszewski, C., Panichi, F., & Szuszkiewicz, E. 2016, *MNRAS*, 455, L104, doi: [10.1093/mnrasl/slv156](https://doi.org/10.1093/mnrasl/slv156)
- Hamann, A., Montet, B. T., Fabrycky, D. C., Agol, E., & Kruse, E. 2019, *AJ*, 158, 133, doi: [10.3847/1538-3881/ab32e3](https://doi.org/10.3847/1538-3881/ab32e3)
- Hara, N. C., Bouchy, F., Stalport, M., et al. 2020, *A&A*, 636, L6, doi: [10.1051/0004-6361/201937254](https://doi.org/10.1051/0004-6361/201937254)
- Jackson, B., Greenberg, R., & Barnes, R. 2008, *ApJ*, 678, 1396, doi: [10.1086/529187](https://doi.org/10.1086/529187)
- Jiang, C.-F., Xie, J.-W., & Zhou, J.-L. 2020, *AJ*, 160, 180, doi: [10.3847/1538-3881/abb01b](https://doi.org/10.3847/1538-3881/abb01b)
- Jontof-Hutter, D., Ford, E. B., Rowe, J. F., et al. 2016, *ApJ*, 820, 39, doi: [10.3847/0004-637X/820/1/39](https://doi.org/10.3847/0004-637X/820/1/39)
- Jontof-Hutter, D., Ford, E. B., Rowe, J. F., et al. 2021, *The Astrophysical Journal*, 911, 154, doi: [10.3847/1538-4357/abf653](https://doi.org/10.3847/1538-4357/abf653)
- Leleu, A., Alibert, Y., Hara, N. C., et al. 2021, arXiv e-prints, arXiv:2101.09260. <https://arxiv.org/abs/2101.09260>
- Lopez, T. A., Barros, S. C. C., Santerne, A., et al. 2019, *A&A*, 631, A90, doi: [10.1051/0004-6361/201936267](https://doi.org/10.1051/0004-6361/201936267)
- Luger, R., Sestovic, M., Kruse, E., et al. 2017, ArXiv e-prints. <https://arxiv.org/abs/1703.04166>
- MacDonald, M. G., & Dawson, R. I. 2018, *AJ*, 156, 228, doi: [10.3847/1538-3881/aae266](https://doi.org/10.3847/1538-3881/aae266)
- MacDonald, M. G., Ragozzine, D., Fabrycky, D. C., et al. 2016, *AJ*, 152, 105, doi: [10.3847/0004-6256/152/4/105](https://doi.org/10.3847/0004-6256/152/4/105)
- Migaszewski, C. 2016, *MNRAS*, 458, 2051, doi: [10.1093/mnras/stw386](https://doi.org/10.1093/mnras/stw386)
- Millholland, S., Laughlin, G., Teske, J., et al. 2018, *AJ*, 155, 106, doi: [10.3847/1538-3881/aaa894](https://doi.org/10.3847/1538-3881/aaa894)
- Mills, S. M., Fabrycky, D. C., Migaszewski, C., et al. 2016, *Nature*, 533, 509, doi: [10.1038/nature17445](https://doi.org/10.1038/nature17445)
- Murray, C. D., & Dermott, S. F. 1999, *Solar System Dynamics* (Cambridge University Press)
- Papaloizou, J. C. B. 2015, *International Journal of Astrobiology*, 14, 291, doi: [10.1017/S1473550414000147](https://doi.org/10.1017/S1473550414000147)
- Papaloizou, J. C. B. 2016, *Celestial Mechanics and Dynamical Astronomy*, 126, 157, doi: [10.1007/s10569-016-9689-9](https://doi.org/10.1007/s10569-016-9689-9)
- Rein, H., Papaloizou, J. C. B., & Kley, W. 2010, *A&A*, 510, A4, doi: [10.1051/0004-6361/200913208](https://doi.org/10.1051/0004-6361/200913208)
- Rivera, E. J., Laughlin, G., Butler, R. P., et al. 2010, *ApJ*, 719, 890, doi: [10.1088/0004-637X/719/1/890](https://doi.org/10.1088/0004-637X/719/1/890)
- Rowe, J. F., Bryson, S. T., Marcy, G. W., et al. 2014, *ApJ*, 784, 45, doi: [10.1088/0004-637X/784/1/45](https://doi.org/10.1088/0004-637X/784/1/45)
- Rowe, J. F., Coughlin, J. L., Antoci, V., et al. 2015, *ApJS*, 217, 16, doi: [10.1088/0067-0049/217/1/16](https://doi.org/10.1088/0067-0049/217/1/16)
- Steffen, J. H., Fabrycky, D. C., Agol, E., et al. 2013, *MNRAS*, 428, 1077, doi: [10.1093/mnras/sts090](https://doi.org/10.1093/mnras/sts090)
- Tamayo, D., Rein, H., Petrovich, C., & Murray, N. 2017, *ApJL*, 840, L19, doi: [10.3847/2041-8213/aa70ea](https://doi.org/10.3847/2041-8213/aa70ea)
- Thommes, E. W., Bryden, G., Wu, Y., & Rasio, F. A. 2008, *ApJ*, 675, 1538, doi: [10.1086/525244](https://doi.org/10.1086/525244)
- Ward, W. R. 1997, *Icarus*, 126, 261, doi: [10.1006/icar.1996.5647](https://doi.org/10.1006/icar.1996.5647)
- Weiss, L. M., Marcy, G. W., Petigura, E. A., et al. 2018, *AJ*, 155, 48, doi: [10.3847/1538-3881/aa9ff6](https://doi.org/10.3847/1538-3881/aa9ff6)